An IRAS/ISSA Survey of Bow Shocks Around Runaway Stars

Dave Van Buren, Alberto Noriega-Cr espo & Ruth Dgani

Infrared Processing and Analysis Center, California Institute of Technology and Jet Propulsion Laboratory, Pasadena, CA, 91125

email: al berto, dave, knill@ipac.caltech.edu

Received —. —.--_.__._——_; accepted _.-. ---.. _____

ABSTRACT

We searched for bow shock-like objects like those known around ζ Oph and α Cam near the positions of 183 runaway stars. Based primarily on the presence and morphology of excess 60 micron emission we identify 56 new candidate bow shocks, for which we determine photometric and morphological parameters. Previously only a dozen or so were known. Well resolved structures are present around 25 stars. A comparison of the distribution of symmetry axes of the infrared nebulae with that of their proper motion vectors indicates that these two directions are very significantly aligned. The observed alignment Strongly suggests that the structures we see arise from the interaction of stellar winds with the interstellar medium, justifying the identification of these far-infrared objects as stellar wind bow shocks.

1. introduction

Infrared bow shocks around nearby runaway OB stars were first discovered by Van Buren and McCray (1988=VM) using IRAS data, There a simple analytic model was developed for the sizes, luminosities and color temperatures based 011 simple momentum balance between the ram pressures of a stellar wind and the radiatively heated dust-bearing interstellar medium. For the prototype objects, the model has 110 free parameters and successful ly reproduces t he fundamental IRA S observables. The model has been extended to describe the axisymmetric kinematics and morphologies of bow shocks (Van Buren et al 1990, Mac Low et al 1991ab, Van Buren and MacLow 1992), primarily those giving rise to cometary ultracompact HII regions.

Bow shocks are a ubiquitous phenomenon. Many stars move supersonically through the ISM and posess winds, satisfying the conditions necessary to give rise to a bow shock. In most cases the wind is too weak, the ISM too tenuous, or the star too faint to yield an observable object, but as observing methodologies improve, more and more will be detected around ever nearer and fainter stars. Detection is no problem though for the bow shocks of runaway OB stars. Their winds arc strong, thus are able to sweep up a large column of interstellar matter, their luminosities are high, giving rise to substantial] heating of the accompanying swept up dust, and a typical fraction (10-2OYO) arc situated in the diffuse ISM where their velocities are supersonic, which supports the generation of such structures. Bow shocks have been found not only around runaway OB stars (Gull and Sofia 1979, VM), but also around cataclysmic variables (Hollis et al 1992), pulsars (Kulkarni and Hester 1988), and stars embedded in molecular clouds (Gull and Sofia 1979, Wood and Churchwell 1989). The heliopause, where the solar wind meets the ISM, is of course the nearest stellar wind bow shock.

We have suspected that bow shocks are common around runaway OB stars ever since

VM found a number around bright, named stars. 'l'his study represents the first systematic assessment of their distribution, targeting a list of known runaway stars with presumed strong stellar winds. Our reasons for identifying the observed structures as bow shocks are:

- They are preferentially found around *high velocity* wind-blowing stars.
- They are aligned with the stars' proper motion vectors.
- '1'heir large-scale properties match the theoretical description of VM for bow shocks observed in the far infrared.

In this paper we justify the first two claims in the context of observational data derived from the IRAS 1 nfrared Sky Survey Atlas[1] (the third claim was demonstrated correct in VM). But our main purpose is simply to present a catalog of a sizeable number of bow shocks for use in characterizing the phenomenon and to provide target objects for future observational and theoretical work.

2. The Sample

There is no systematic or complete list of runaway stars. We chose our target list from the catalogs of Garmany, Conti and Chiosi (1 982), and Cruz-Gonzales et a] (1 974), ant] the list of runaway stars by Stone (1 979). Stars were selected on the basis of their radial and space velocities: generally stars with peculiar space motions greater than 30 km/s were considered runaways. Our list should not be considered systematic or complete since it inherits the biases of the input catalogs. The Hipparcos results will supply us within a few

[1] The ISSA is a machine-readable atlas of the sky in the four IRAS bands at 12, 25, 60 and 100 μm at 5 arcminute resolution.

years with a more complete and unbiased catalog of runaway stars. Given the anticipated availability of the Hipparcos sample, and the biased and incomplete nature of existing data, we did not deem it worthwhile to cull the literature for all possible runaway stars.

We also chose a separate control sample of 30 stars, not thought to be runaways, from the input lists. The sample size is 30 because it allows a statistically significant test of whether the observed incidence of associated far-infrared emission in the runaway sample is different than from that in an otherwise mostly similar non-runaway sample. There is one difference between the two samples that should be mentioned: the control sample is missing the bright end of the apparent magnitude distribution that the runaway sample has. We interpret this simply to mean that the OB stars closest to a typical location (like ours) far from star forming regions are in fact runaway stars, ie those that have left their original locations at high velocity and now comprise a "(field" population.

3. Survey Methodology

3.1. Collecting the Data

The IRAS data was extracted from the on-line archive maintained at the Infrared Processing and Analysis Center[2] in the following manner. Software was developed to access the ISSA Postage Stamp Server (URL="http://astrovr.ipac.caltech.edu:8888/ISSA-PS") at IPAC. This "survey engine" takes a list of object *names* and automatically makes a postage stamp request for each target. The request responses are received as HTML documents containing URLs to the prepared FITS files of extracted 2° x 2° fields. The 4 FITS files representing the 4 IRAS bands at 12, 25, 60 and 100 μm are transferred automatically

[2]IPAC is funded by NASA as part of the IRAS extended mission under contract to JPL.

to local storage for analysis. This technique allows the data collection for surveys to be undertaken from large image databases with minimal effort.

3.2. The Excess Maps

We identify targets as bow shock candidates if they have associated far infrared nebulae. Diffuse emission is associated if it is at or near the target position and if it shows evidence of heating by a source at the target's location. We determine heating by creating "excess maps" which show the distribution of material whose color temperature is different from the background galactic cirrus emission.

We use the 100 μm image as the base image from which the 12, 25 and 60 μm excesses are to be computed. They are computed by masking out the central 10 of the images and producing pixel-by-pixel scatter diagrams of the 12 vs 100, 25 vs 100 and 60 vs 100 μm maps. In these plots we use the lowest. 50% of the 100 μm points to define a linear relation between the surface brightnesses in each band. An example is shown as figure 1. We then use these relations to subtract the 100 μm based background from entire images. Each pixel in the resulting images now corresponds to the excess (or deficit) emission above that expected from the mean background relation between the two bands. This method of background removal is insensitive to zero-point errors and strong backgrounds, unlike techniques using band ratios or color temperatures.

3.3. The Bow Shock Candidates

A target becomes a candidate when the 60 μm map shows a clear excess near the target position. In some cases a well resolved arcuate nebula is present, but often the 'excess is only slightly or uII-resolved. The 60 μm images of the 56 candidates are shown in figure 2.

Catalog and derived data for the candidates are presented in table 2, which is organized in the following way: the first four columns give name, spectra] type, right ascension and declination (J2000) of the runaway stars, respectively, Columns (5) and (6) contain the galactic coordinates and column (7) the apparent visual magnitude. Column (8) is the position angle of the bowshock symmetry axis. We describe how this measurement is made in a subsequent section. A rough morphological classification following the nomenclature of VM is given in column (9). Columns (10) - (13) are the IRAS measured fluxes in Janskys for bowshock emission at 12, 25, 60 and 100μm, respectively, with the notation 10.0 = 1.0+1. The far infrared fluxes are based on the "excess maps" and take into account all the apparent emission above the local background. Column (14) gives the distance from the star to the peak intensity as measured in the 60μm "excess map" in arc minutes. Columns (15) and (16) are the proper motions in arcseconds per year compiled from the 'Hipparcos Input Catalogue' (1992). We direct readers to that source for the original references. 'J)he last column, (1 7), is the radial velocity in km s^{-1} compiled from "The Bright Star Catalogue" (Hoffleit, 1982), or from the Simbad data base in some cases. Some of these stars are likely spectroscopic binaries, with single (S1 31) or double (SB2) lined spectra. Orbit determination is designated by the O suffix (e.g. SB2O). The V and V? suffixes refer to variable and/or suspected variable stars. The suffixes A, B, C and D arc quaility index (Cruz-Gonzalez et al. 1974) which reflect the uncertainty in the velocities (4, 6, 9 and 20 km s^{-1}, respectively).

3.4. Runaway and Non-Runaway Control Samples

The control sample was chosen to be a random set of non-runaway stars taken from the same catalog sources as the runaway stars. The motivation was primarily to be able to distinguish whether the 56/183 $\approx$ 0.3 ratio of far infrared excess stars seen in the runaway

sample is measurably different from the fraction of of non-runaway stars with excesses. A 3σ measurement of the ratio 0.3 requires a sample size of about 30 objects, ie the binomial distribution standard deviation $\sigma = \sqrt{30(0.3)(1-0.3)} = 2.6$.

Before moving 011 to the excess fraction in the non-runaway sample we now examine the differences in the catalogued properties of the two groups of stars just to verify that it is reasonable to call one the runaway sample and the other the non-runaways.

The distribution) of apparent magnitudes for the runway sample (56 stars) has a mean value $\widehat{m_v} = 6.1$ mag and a dispersion $\sigma = 2.0$ mag. The controlsample (30 stars) is slightly fainter, $\widehat{m_v} = 7.0$ mag, with a dispersion $\sigma = 1.3$ mag. The main difference is at the bright magnitude end. The runaway sample has well kuow bright objects with bowshocks, e.g. δ Sco (HD 143275) and ζ Oph (HD 149757), but the control doesn't have any bright, stars. The most likely astrophysical] explanation is that the bright OB stars near to us have already left their natal associations, so they are runaways.

The distribution of radial velocities is even more compelling (see Fig 3). The runaway sample has a mean V_r :--0.3 km s^{-1} and a dispersion o = 30.1 km s^{-1}, while the non-runaway sample has a mean V_r = -1.9 km s^{-1}, but a dispersion σ = 5.3 km s^{-1}, i.e. the runaway velocity dispersion is nearly 6 times wider. This is not surprising since we selected the samples with such characteristics, nevertheless, it stresses the importance of the velocity to discriminate runaway stars. In view of the next paragraph in fact, with current data radial velocities are by far a better discriminant than proper motions. We expect the situation to improve with 1 Hipparcos measured proper motions in the next few years.

The distribution of proper motions arc surprisingly similar, i.e. the means and dispersions are not significantly different, but the main caveat is the large uncertainties of the proper motions themselves. The mean values of the proper motions for the runaway in both directions are -5.9 and -1.2 mas/yr, with dispertions of 12.4 and 14.4

mas/yr, respectively. For control sample the mean values are -1.1 and -1.8 mas/yr, with corresponding dispersions of 12.3 and 9.5 mas/yr.

Excess far infrared emission was found associated with 4 of the 30 non-runaway stars in the control sample. Standard statistical techniques applied to this fraction show that the proportion of non-runaways with excesses is different from the proportion of runaways a the 970/0 confidence level (56/183 vs 4/30). Wc thus conclude that the infrared excesses are a property of the space motion of the runaways, consistent with the hypothesis that the excess arises from radiatively heated dust near the stars - dust associated with gas penetrating close to the star because of its high rain pressure. Ordinarily, for a low velocity (subsonic) star, we expect that the combined action of stellar winds and radiation pressure will eject interstellar dust from the neighborhoods.

4. Distribution of Symmetry Angles versus Proper Motions

A resolved transverse bow shock has a wc] l-defined paraboloid] shape with the star located on the symmetry axis. We want to determine the symmetry axis objectively, without relying on eye measurements.

The symmetry angles for the resolved bow shocks were determined in an objective manner by finding the: best fit axis for reflection symmetry (constrained to pass through the star) for cliffc.rent isophotal contours as a function of surface brightness. We used the 60 μm excess maps because they are very much more free of confusing background structure than the original ISSA images. The conceptual procedure for determining the symmetry axes goes like this: each contour C is used to generate a 2 dimensional function S whose value is 1 inside the contour and 0 outside. At each position angle s for a test symmetry axis the isophotal shape is reflected through the symmetry axis to form a new function S' defined similarly to S. The integral $O = \int$,$S" is now a measure of the overlap of S and S'. The

angle which maximizes the overlap is the best fit symmetry axis. We show in figure 4 plots of O vs s for a number of isophotal contours in the 60 μm excess maps of four objects. It is easy now to choose by eye which of the 2 (or 4) possibilities corresponds to the oriented symmetry axis without fear of subjectivity. Some care must be taken here when working with the postage stamp images since they are not always oriented so that celestial north is directly toward the top of the image. The uncertainties in the angle measurements are of order 10°, but we do not have a statistic to be more precise.

The direction of motion of the stars is determined from the orientation of their proper motions (a few mas/yr for most stars). At present the uncertainties in the proper motions are as large as the measured values for $\sim 90\%$ of the selected stars, and we consider this the main source of error in the following analysis.

4.1. Directional Analysis

The direction of motion through the ISM of the star should coincide with the orientation of the symmetry axis if the bow shock hypothesis holds. But even in cases where the proper motions are known the local relative velocity of the star and the ambient gas are not. For stars within a few kpc, which is true of our sample, the galactic shear is relatively small compared to the runaway stars' velocities so we have not corrected for galactic rotation. In some cases we may have misidentified a part of an unrelated filament or a bubble as a bow shock since the morphological classification is subjective. Not the least of all uncertainties are the rather large errors in the proper motion vectors themselves, and the smaller uncertainties in the symmetry axis orientations.

In Table 4 we show the relative angles in degrees between the orientation of the far infrared symmetry axes and the proper motions of the star for 25 cases where the proper motion are known. The second column shows the errors in degrees calculated as the sum of

the error in the direction of the proper motion and the error in determining the direction of the bow shock. A relative angle of 0° means that the proper motion is coincident with the geometrical direction of the bow shock.

The techniques developed for analyzing directional data are different from the more familiar techniques used for linear data. Let 01,. . . ,0,, be the values of the relative angles (in our case $n = 25$). Applying the standard procedure (Madria 1972), we assign to each angle a unit vector in this direction. Let the vector sum of these unit vectors divided by n be $\mathbf{R}$ (the vector average) and let R be its length. The mean direction is defined as the direction of $\mathbf{R}$ and the circular variance is defined as $S_0 = 1 - R$. Note that these definitions are rotationally invariant as desired. The circular variance is zero when all the points are identical and it is one when they are uniformly distributed on the circle. The angular standard deviation in radians is given by $s_0 = \sqrt{-2\log(1 - S_0)}$.

Applying the procedure above, we find that the simple average angle is 8° and the standard deviation 75°. We then determine a weighted average, weighting each point inversely with the square of the error in the proper motion position angle. The weighted average angle is 3° the standard deviation 60". In both cases the average angle is less than or the of order of $\sigma/\sqrt{(N - 1)}$ away from O°.

We present a "rosette diagram') of the relative angle distribution in Fig. 5, grouping the data from '~'able 4 in 45° intervals. Corresponding to each interval we construct a sector with apex at the origin radius proportional to the class frequency (the number of angles in that interval). It is clear that the distribution of relative angles is strongly biased towards the zero direction.

Finally we apply Kuiper's test (Kuiper 1960) to test whether the coincidence between the bow shocks and the proper motions direction could have arisen by chance. In other words what is the probability that these points are derived from the uniform distribution.

Since we have a small sample we used a Kolmogorov-type test that was adjusted to the circular case by Kuiper. If $U_n(\theta)$ is the empirical distribution function and $F(\theta)$ is the assumed distribution function (in our case $F(\theta)=\theta/2\pi$ the uniform distribution) then the statistic

$$V_n = D_n^+ + D_n^- \tag{1}$$

where

$$D_n^+ = max(U_n(\theta) - F(\theta)) \tag{2}$$

$$D_n^- = \max(F(\theta) - U_n(\theta)) \tag{3}$$

is a lnea.sure of the deviation between the empirical distribution and the assumed one. It is rotationally invariant, i.e. does not depend on the choice of the zero direction. The statistic $V_n' = \sqrt{n}V_n$ *is* tabulated in Madria (1 972). The 5 °/o value of V_n' is 1.67, our value is 1.88, so wc reject the hypothesis of uniformity at the 95% confidence level. The Kuiper test for our data shows that the distribution] is highly non uniform as can be seen from the "rosette diagram". Together with the fact that the average direction is within one standard deviation from the zero direction this is consistent with the hypothesis that the observed structures around runaway stars arise as a consequence of the confinement of their stellar wind by the lSM due to their supersonic motion.

5. Acknowledgements

A. N.-C. and D. V.B. research is supported by NASA Long Term Astrophysics program through a contract with the Jet Propulsion Laboratory (J 1'1,) of the California Institute

of Technology. R.D. thanks the Swiss National Foundation for its support and the visiting scientist program at JPL. The IRAS mission was made possible by the taxpayers of the U. S., U .1<., and the Netherlands. This research has made use of the Simbad database, operated at CDS, Strasbourg, France. We thank Susan Terebey, Vicky Kaspi, and Joseph Mazzarella for useful conversations.

REFERENCES

Cruz-González, C., Recillas-Cruz, E., Costero, R., Peimbert, M., & Torres-Peimbert, S. 1974, RMxAA, 1, 211

Garmany, C.D., Conti, P.S., & Chiosi, C. 1982, ApJ, 263, 777

Gull, T.R., and Sofia, S. 1979, ApJ, 230, 782

Hollis, J., Oliversen, R.J., Wagner, R.M., and Feibelman, W.A. 1992, ApJ, 393, 217

Kuiper, N.H. 1960, Nccl.Akacl.Wet.Proe, A63, 38

Kulkarni, S., and Hester, J.J. 1988, Nature, 335, 801

Mac Low, M.M., Van Buren, D., Wood, D.O. S., & Churchwell, E. 1991a, ApJ, 369, 395

Mac Low, M. M., Van Buren, D., Wood, D.O. S., and Churchwell, E. 1991b, ApJ, 269, 395.

Madria, K.V. 1972, "Statistics of Directional Data" (Academic Press, London)

Stone, R. 1979, ApJ, 232, 520

Van Buren, D., & McCray, R. 1988, ApJ, 329, L93

Van Buren, D., Mac Low, M.M., Wood, D.O. S., and Churchwell, E., 1990, ApJ, 353, 570.

Van Buren, D., and Mac Low, M. M., 1992, ApJ, 394, 534

Wood, D.O.S, and Churchwell, E 1989, ApJS, 69, 831

This manuscript was prepared with the AAS LaTeX macros v3.0.

Figure Captions

Figure 1. Conflation of 25 vs 100 μm and 60 vs 100 μm pixel intensities for the 2-degree region around HD 188001 in the ISSA images. We fit a linear relation to the *lowest* 50% of the 100 μm points and use that relation to construct excess maps. The region around the object of interest is excluded from the fit. Note that excess maps are much better than ratio maps because there are significant zero-level offsets in each band and because they have the same units as the original maps.

Figure 2. 60μm excess maps for likely bowshocks around runaway stars. Each field is 2° x 2° and darker means a larger excess. Some images have residual stripes clue to uncalibrated gain drifts in the IRAS detectors (which in fact were not designed for imaging). From the top, left to right: HD 1337, HD 2905, HD 4142, & HD 17505.

Figure 2 (continued) From the top, left to right: HD 19374, HD 19820, HD 22928, & HD 24431.

Figure 2 (continued) From the top, left to right: HD 30614, HD 34078, BD+39 1328, & HD 36862.

Figure 2 (continued) From the top, left to right: HD 37020, HD 37737, HD 41161, & HD 41997.

Figure 2 (continued) From the top, left to right: HD 42933, HD 47839, HD 48099, & HD 50896.

Figure 2 (continued). From the top, left to right: HD 52533, HD 54662, HD 64315, & HD 66811.

Figure 2 (continued). From the top, left to right: HD 89137, HD 92206, HD 101131, & HD 112244.

Figure 2 (continued). From the top, left to right: 111) 130298, 11 D 135240, HD 329905, & HD 143275.

Figure 2 (continued). From the top, left to right: HD 171491, HD 175514, HD 186980, & 111) 188001.

Figure 2 (continued). From the top, left to right: HD 227018, HD 189957, HD 192163, & 111) 195592.

Figure 2 (continued). From the top, left to right: BD+43 3654, HD 199579, HD 202214, & HD 203064.

Figure 2 (continued). From the top, left to right: BD+43 3654, HD 199579, HD 202214, & HD 203064.

Figure 2 (continued). From the top, left to right: HD 203467, HD 207538, HD 210839, & 111) 212593.

Figure 2 (continued). From the top, left to right: HD 213087, HD 214680, BD+63 1964, & HD 224151.

Figure 3. Distribution of radial velocities for the bowshock (top) and non-runaway control (bottom) samples. Radial velocity is a much better discriminant for runaway vs non-runaway than proper motions because of significantly large astrometric errors. We await the Hipparcos results to bring higher accuracy to the stellar proper motions.

Figure 4. Depiction of the symmetry angle (counter-clockwise and uncorrected) determination for the bowshocks detected using the 60μm excess maps. The angular marks are every 10° (see text for details). From the top, left to right: HD 149757 (200), HD 192163 (30s°), HD 188001 (145°) & HD 48099 (700).

Figure 5. 1 distribution of the relative angles, obtained from the difference between the symmetry bowshock angle and the orientation of its motion determined from the star's proper motion. The binsize corresponds to 45°.

TABLE 1

RUNAWAY STARS

HD 108	HD 1337	HD 2905	HD 4142	HD 7927
HD 12993	HD 13268	HD 14633	HD 14947	HD 15558
HD 16691	HD 17505	HD 17506	HD 19374	HD 19820
HD 20218	HD 22928	HD 24431	HD 24912	HD 30614
HD 34078	HD 35921	HD 36861	HD 36862	HD 37020
HD 37022	HD 37043	HD 37737	HD 38666	HD 39478
HD 39680	HD 41161	HD 41534	HD 41997	HD 42933
HD 46966	HD 47839	HD 48099	HD 50896	HD 51480
HD 51547	HD 52089	HD 52533	HD 54662	HD 57060
HD 60369	HD 64315	HD 66811	HD 69106	HD 74194
HD 78584	HD 89137	HD 92206	HD 92504	HD 92554
HD 93161	HD 93845	HD 94663	HD 95275	HD 96670
HD 97991	HD 101131	HD 101298	HD 104200	HD 109399
HD 109978	HD 110946	HD 112244	HD 112484	HD 115071
HD 116852	HD 122879	HD 123008	HD 124195	HD 125206
HD 130298	HD 135240	HD 135591	HD 135742	HD 143275
HD 144695	HD 145217	HD 146628	HD 148937	HD 149038
HD 149363	HD 149757	HD 150136	HD 150197	HD 150958
HD 151397	HD 151515	HD 151804	HD 152246	HD 152408
HD 152723	HD 156212	HD 156292	HD 157857	HD 158186
HD 158926	HD 160641	HD 160730	HD 164019	HD 167264
HD 167330	HD 167633	HD 168941	HD 169582	HD 170452
HD 171198	HD 171491	HD 171635	HD 173820	HD 175514
HD 186980	HD 188001	HD 188209	HD 189957	HD 190918
HD 191765	HD 192103	HD 192163	HD 192281	HD 192639
HD 193077	HD 193514	HD 193576	HD 195592	HD 195907
HD 197419	HD 199579	HD 201345	HD 201910	HD 202214
HD 203064	HD 203467	HD 206859	HD 209481	HD 209952
HD 209975	HD 210745	HD 210839	HD 212593	HD 213087
HD 214930	HD 214993	HD 216534	HD 217476	HD 218376
HD 218915	HD 219286	HD 223047	HD 223385	HD 224151
HD 227018	HD 227877	HD 235807	HD 235825	HD 237019
HD 240165	AGK +29 2199	AGK +43 513	AGK +59 292	AGK +60 1562
BD +13 4091	BD +39 1328	BD +43 1102	BD +45 3260	BD +59 186
BD +60 169	BD +61 2550	BD +62 338	BD +63 1964	CPD -54 6791
CPD -60 2454	CPD -60 2457	CPD -61 2030	CPD -61 2033	CPD -61 2043
CPD -61 2078	CPD -61 2163	CPD -61 2118		

CONTROL STARS

HD 34656	HD 35619	HD 52266	HD 75821	HD 76556
HD 78344	HD 90087	HD 91572	HD 92714	HD 93250
HD 93843	HD 96670	HD 97253	HD 105627	HD 155775
HD 155806	HD 156134	HD 156154	HD 159176	HD 164492
HD 165052	HD 165246	HD 167263	HD 167971	HD 169755
HD 190864	HD 193322	HD 206267	HD 237090	HD 254755

TABLE 2

RUNAWAY STARS AND BOWSHOCK PROPERTIES

(1) Star	(2) ST	(3) α_{2000}	(4) δ_{2000}	(5) l	(6) b	(7) m_v	(8) PA (°)	(9) Type[a]
111)1337	O9IIInn+.	001742.99	+51 2559.3	117.59	-11.09	6.14	73	⊃
HD2905	B1 lac	0032 59.87	+6255 54.65	120.84	+0.14	4.16	77	⊃
111)4142	B5V	0044 26.41	+47 51 50.2	121.72	-14.99	5.67		•
111)17505	O6c	0251 07.99	+60 2502.9	137.19	+ 0.90	7.10	244	⊃ -)
111)19374	B1.5V	030725.68	+ 175247.7	162.98	-34.?1	6.11	-	•
111)19820	O9IV	031405.31	+59 3348.6	140.12	+1.54	7.11	7	⊃
111)22928	B5III	034255.29	+47 4716.9	150.28	-5.77	2.99	100	⊃
HD24431	091 V-V	035538.42	+52 3828.3	148.84	-0.71	6.73	250	⊃
HD30614	O9.5Iac	045402.97	+66 2033.4	144.07	+14.04	4.29	339	⊃
111)34078	O9.5Ve...	05 16 18.15	+3418 41.6	172.08	-2.26	5.94		•
BD+39 1328	O9III:	05 32 13.80	4400357.9	169.11	+ 3.60	9.84		•
HD36862	B0.5V	053508.40	+09 5606.0	195.05	-11.99	5.61	290	⊃
11D37020	0 7	05 35 15.70	-052311.0	209.01	-19.39	6.73		•
III)37737	B0II:	054231.07	+36 1200.8	173.46	+ 3.24	8.00		○?
111)41161	O8V	0605 52.47	+ 48 14 57.8	164.97	+12.89	6.77	285	⊃
111)41997	O7	06 0s 55.77	+15 4218.7	194.14	-1.98	8.41		•
111)42933	B3III+	061017.90	-54 58 07.5	263.30	-27.68	4.81		•
11[)47839	O7Ve	064058.62	+09 5344.7	2(02.94	+ 2.20	4.66		•
111)48099	O6c	0641 59.20	+06 2042.7	206.21	+ 0.80	6.35	70	⊃
HD50896	W N	0654 12.97	-23 55 42.0	234.76	-10.08	6.91		○
HD52533	O9V	0701 26.98	-030703.7	216.85	+ 0.80	7.72		● -)
HD54662	O7III	070920.22	-102049.4	224.17	-0.78	6.21	320	⊃
111)64315	O6c	075220.28	-26 25 46.6	213.16	+ 0.36	9.16		•
HD66811	O5Ia...	080335.14	-400012.0	255.98	-4.71	2,20		)?
111)89137	B2II	10 15 39.96	-5115 25.2	279.69	+ 4.45	7.98	333	⊃
111)92206	O6	103722.24	-583723.1	286.22	-0.17	7.60	256	•
}11)101131	0711	11 3748.38	-631923.2	294.78	-1.62	7.16	176	⊃
111)112244	O9Ibc	125557.04	-565008.5	303.55	+ 6.03	5.32		•
111)130298	O5/O6	144933.77	-5625 37.9	318.77	+ 2.77	9.27		)?
111)135240	O8.5V	15 16 56.76	-605726.0	319.69	-2.91	5.10	235	⊃
111)329905	O+...	154754.50	-483746.0	3'30,42	+4.59	10.45		•
111)14327S	B0.2IV	160019.96	-2237 16.7	350.10	+22.49	2.30	195	⊃
111)149757	O9V	163709.40	-103402.8	6,28	+23.59	2.60	20	⊃
111)156212	O+...	171727.48	-274601.4	357.59	+5.83	7.91	270	⊃ -)
HD158186	O9.5V	172912.69	-31 3.204.7	355.91	+1.60	7.00		•
111)169582	O5c	182543.03	-0945 11.2	21.33	+1 .20	8.70		•
111)171491	B5	183508.06	+00 0234.4	31.11	+3.65	8.30	100	⊃
111)175514	O8:Vnn	185523.06	+09 2048.2	41.71	+3.38	8.59	10	⊃
111)1/76980	07.5111.,	194615.83	+32 0658.2	67.39	+3.66	7.48	-	• -)?
111)188001	O8c	19.5221.67	+18 40 19.3	56.48	-4.33	6.23	145	⊃
HD227018	0 7	195949.02	+35 1833.9	71.58	+ 2.87	9.25		•
111)189957	B0III	200059.91	+42 0031.3	77.43	+6.17	7.82		•
111)192163	WNn...	201206.43	+38 21 17.3	75.48	+ 2.43	7.48	308	
111)195592	O9.5Ia	203034.85	+44 1854.2	82.36	+2.96	7.08	310	o?'- ⊃
BD+43 3654	B	203335.90	+43 5906.0	82.41	+ 2.33	11.5	345	⊃
111)199579	O6Ve	205634.67	+44 5529.4	85.70	-0.30	5.96		•
111)202214	B0II	21 11 48.15	+59 5911.6	98.52	+ 7.99	5.64		)
111)203064	O8c	21 1827.05	+ 435645.8	87.61	-3.84	5.00		•
HD203467	B3Ve	21 1922.10	+64 5218.3	102.74	+10.69	5.18		•
111)207538	B0V	21 4739.67	+59 4202.3	101.60	+ 4.67	7.31		•
111)210839	O6Iab:...	2211 30.60	+59 2452.7	103.83	+ 2.61	5 .06	222	⊃
111)212593	B9Iab	222430.91	+49 2835.2	99.90	-6.71	4.56		•
HD213087	B0.5Ibc...	222705.28	+65 0756.6	108.50	+6.39	5.52	90	⊃
111)214680	O9V	223915.60	+39 0301.2	96.65	-16.98	4.90	100	⊃
BD+63 1964	B0II	231721.42	+ 64 0716.6	112.89	+3.10	8.46	297	⊃
111)224151	B0.5IIvar	235533.71	+57 2443.7	115.44	-4.64	6.00		•

[a] ⊃= bowshock, ○=bubble,)= shell, • = excess

TABLE 2

RUNAWAY STARS AND BOWSHOCK PROPERTIES (CONTINUED)

(1) Star	(10) $F_{12\mu m}$[a]	(11) $F_{25\mu m}$	(12) $F_{60\mu m}$	(13) $F_{100\mu m}$	(14) r_p[c]	(15) pm_x[d]	(16) pm_y	(17) V_r[e]
111)1337			1.0+1	2.6+1	12.1	+0.014±4	+0.001±4	-35SB2O
111)2905	5.3+o	3.1+1	1.6+2	7.6+1	6.0	+0.001±1	+ 0.0034-1	-2
111)4142		6.01	5.4+0	1.3+1		-0.02746	+ 0.0204-4	-60SB
111)17505		1.5+2	7.4+2	2.0+3	10.1	+0.010±5	-0.0094-5	-17
111)19374			8.3+0	2.8-I- I		-0.02643	+0.010±3	+21SB
111)19820			3.0+3			-o 004±3	+0.002±3	-4C
HD22928	2.6+o	5.0+o	8.5+1	1.1+2		+0.028±4	-0.034±4	+4
111)24431	5.3-1	2.'740	7.1+1		7.6	+0 000+3	+0.004±3	-I OH
111)30614	8.0 1	4.5+1	3.1+2	4.7+2	12.8	+0.000±4	+0.005±4	+6V?
111)34078	2.9+1	3.0+2	7.6+2	1.4+3		-0.012410	+ 0.03149	+ 59V
BD+39 1328			1.240					-72
111)36862	1.4+0	4.2+0	1.6+2	3.3+3	14.2	-0.00144	-0.007±4	+36V?
111)37020	5.5+3	7.0+4	1.8+5	3.5+5				+32SB
111)37737			1.8+2			-0.015414	-0.002±11	-251)
HD41161		1 .1+0	9.0+0	5.5+o	3,0	-0.01149	-0.002 ±8	+5
111)41997	4.8+0	2.1+2	1.0+3	2.1+3				-181)
111)42933	1.4-1	2.1+0	1.6+1	1.6+1		-0.003±4	+ 0.00544	+31
111)47839		7.1+1	9.5+2	4.5+3		+0.001±2	-0,00742	+33SB
111)48099		3.7+1	2.2+2	1.5e+2	1.5	+0.006±5	+0.005±5	+31V
111)50896	5.4-1	2.9-1	1.3+2	9.9+1		-0.00144	-0.00234	+1 000
111)52s33			4.4+1	2.5+2		-0.003± 25	-0.007425	6B
111)541X2		4.8+1	4.8+2	8.1+1	6.7	+0.007±15	-0.019415	+58
111)64315		2.8+2	3.1+3	7.6+3				28
111)6681 1	2.4+0	1.2+0	1.6+0			-0.03142	+0.01 1+2	-24V?
111)89137		8.0-1	3.9+1	7.6+1		+ 0.00144	+ 0.00444	+3C
111)92206		1.1+3	4.7+3	1.0+ 4		+ 0.000415	-0.0134-11	-10C
111)101131		4.7+2	1.3+3	9.7+o	6.2	-0.01447	-0.011±7	-8D
111)112244		5.5+0	6.2+1			-0.021±25	-0.022425	+18V
111)130298		7.1+1	8.6+1	4.7+1				-741)
111)135240			2.5+2		11.7	-0.013410	-0.011± 10	+9SBO
111)329905		3.1+0	3.9+1	4.4+1				+15C
111)143275	2.9+o	1.4+2	8.4+2	5.7+2	6.4	-0.01244	-0.022±4	-7
111)149757	3.2+1	7.1+2	2.9+ 3	3.5+3	4.2	+0.0009±4	+0.026±1	-15V
111)156212			3.0+ 1	1.3+2	8.3	-0.00345	-0.00245	-46
111)158186		3.5+1	I .742			-0.027312	-0.02049	+44:
111)169582		8.8+o	9.3+1					-13.5
111)171491		7.84-0	3.1+2	6.1+2	4.5	-0.01244	-0.01644	-20
111)175514		7.50+0	3.2+ 2		4.5	+0.006±5	+ 0.0054-5	+29D
111)186980		1.2+1	4.1+1			+0.009±8	-0.01 9±8	+4C
111)188001		1.8+o	4.5+1		4.2	-0.00544	-0.01244	+9SB
111)227018		1.2+2	9.6+2	2.2+3		-0.013±9	-0.008±8	+ 15V?
111)189957		2.4+0	2.0+1			-0.0164-32	+ 0.017418	+43C
111)192163		5.6+1	2.7+ 2	7.8+1	5.4	-0.00742	-0,01032	+1 000
111)195592		5.0+2	1.7+3		6.4	+0.002±4	-0.004±4	-28
BD+43 3654	2.4+1	9.9+2	5.9+3	2.3+3	6.4			
111)199579		8.5+1	2.5+2			-0.00946	+0.011±5	-6SBO
111)202214		1.6+1	6.3+1			-0.009,14	+0.011±4	-16
111)203064		1.0+2	3.7+2	3.3+2		-0.00143	-0.00643	+1SB
111)203467	7.4+o	1.6+1	1.5+2	1.6+2		+0.006±4	+0.004±4	-17
111)207538			7.84-0:			-0.01746	+ 0.016±6	-15
HD210839	1.2+0	1.2+2	3.5+2	1.1+2	5.4	-0.00235	-0.00635	-74V?
111)212593			2.0+0	2.3+1		-0.010±4	+0.001±3	-26
111)2130S7			8.4+1			+0.001± 2	-0.00242	-] 5V
HD214680		2.2+1	8.6+1	2.0+1		+0.001±1	-0.00541	-10V?
BD+63 1964			2.5+1			-0.02345	-0.00245	-125V
111)224151		4.2+0	2.0+1			-0.001 ±7	+0.018±7	-26SBO

[b] Integrated fluxes in Jy

[c] r_p=distance from star to peak intensity in arcminutes

[d] pm_x & pm_y in arseconds per year

[e] V_r in km s^{-1}

TABLE 3

CONTROL STARS

(1) Star	(2) ST	(3) α_{2000}	(4) δ_{2000}	(5) Z(pc)	(6) n_{ω}^{a}	(7) V_r	(8) pm_x	(9) pm_y[a]
HD 237090	B0.5IV:nn	03 15 10.84	+59 54 42.7	77	9.01	-6A	+0.002±7	-0.010±7
HD 34656	O7e...	05 20 43.00	+37 26 18.9	13	6.79	+0C	-0.001±15	-0.010±11
HD 35619	O7	05 27 36.07	+34 45 19.8	-3	8.57	-1C	+0.005±10	-0.007±9
HD 254755	O9Vp	06 18 31.73	+22 40 45.3	72	8.84	+9C		
HD 52266	O9V	07 00 21.05	-05 49 36.7	-15	7.23	+5D	-0.001±14	-0.020±12
HD 75821	B0III	08 50 33.43	-46 31 45.0	-37	5.10	+7E	-0.009±25	-0.006±25
HD 76556	O+...	08 55 07.05	-47 36 27.6	-57	8.20	+0A	-	-
HD 78344	O+...	09 05 51.30	-47 46 05.0	-15	9.01	-5D	-	-
HD 90087	B3III	10 22 20.80	-59 45 19.7	-49	7.80	-2C	-0.024±12	-0.010±9
HD 91572	O7	10 33 12.32	-58 10 12.7	-3	8.20	-	+0.005±5	+0.014±14
HD 92714	O5?	10 41 03.80	-58 34 12.0	11	9.40	+3E		
HD 93250	O7	10 44 45.13	-59 33 54.2	-30	7.40	+15E	+0.002±11	-0.002±9
HD 93843	O6IIIe...	10 48 37.77	-60 13 25.2	-48	7.33	-9A	-0.009±14	-0.008±12
HD 96670	O7	11 07 13.78	-59 52 22.9	15	7.42	+2A	-0.034±16	+0.002±17
HD 97253	O5e	11 10 42.05	-60 23 03.6	4	7.11	+1E	-0.004±12	-0.004±9
HD 105627	O9V	12 09 44.63	-62 34 54.1	-3	8.12	+2D		
HD 155775	B1III	17 15 22.12	-38 12 46.2	3	6.72	-3D	-0.002±16	-0.010±13
HD 155806	O8Ve	17 15 19.15	-33 32 54.2	51	5.53	+4C	+0.010±6	-0.001±5
HD 156134	B0Iab...	17 17 20.80	-35 32 54.3	65	8.05	-6E	-	-
HD 156154	O+...	17 17 27.09	-35 32 11.2	62	8.07	-	-	-
HD 159176	O6V+...	17 34 42.39	-32 34 54.1	1	5.68	-4B	+0.005±25	-0.010±25
HD 164492	O6	18 02 23.43	-23 01 50.1	-6	7.30	+1A	+0.001±25	+0.005±25
HD 165052	O+...	18 05 10.46	-24 23 54.9	-41	6.86	+3C	+0.003±25	-0.010±25
HD 165246	O9III:	18 06 04.59	-24 11 44.2	-37	7.72	-	+0.012±18	-0.016±18
HD 167263	B0.5Ib	18 15 12.85	-20 23 16.6	-33	5.95	-4C	-0.003±25	-0.003±25
HD 167971	O9...	18 18 05.76	-12 14 32.8	41	7.50	+1C	-0.013±11	+0.012±8
HD 169755	B4Ib:	18 26 48.60	-14 29 57.0	-35	9.26	+6D	-	-
HD 190864	O7IIIe...	20 05 39.75	+35 36 29.2	77	7.76	-2C	-0.009±15	+0.020±11
HD 193322	O9V	20 18 06.92	+40 43 55.8	54	5.82	-7C	-0.003±25	-0.004±25
HD 206267	O6...	21 38 57.54	+57 29 20.7	53	5.62	-8A	-0.005±1	+0.000±1

TABLE 4

BOWSHOCK RELATIVE ANGLES

Objects	Relative Angle (c)	Error (")
111) 101131	5	52
111) 149757	18	11
HD 48099	20	54
HD 210839	24	100
BD+ 631964	32	26
HD 156212	34	180
HD 2905	59	180
111) 19820	70	82
HD 92206	76	92
111) 36862	102	62
HD 192163	104	19
HD 17505	112	38
HD 195592	156	127
111) 54662	160	93
HD 171491	237	26
HD 214680	291	26
111) 213087	297	100
HD 18801	302	36
HD 101131	305	41
111) 89137	319	114
111) 22928	320	20
111) 175514	320	55
HD 30614	339	86
HD 143275	346	20
HD 1337	347	32

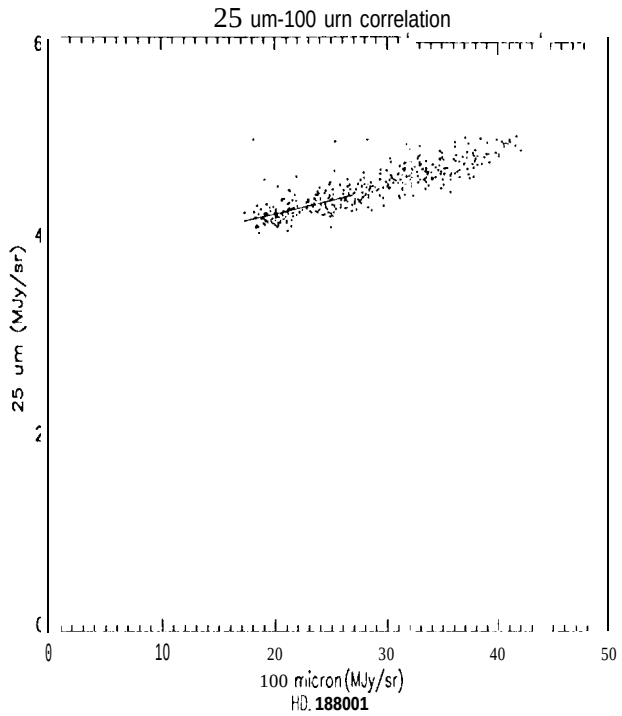
25 um-100 urn correlation
25 um (MJy/sr)
100 micron (MJy/sr)
HD. 188001

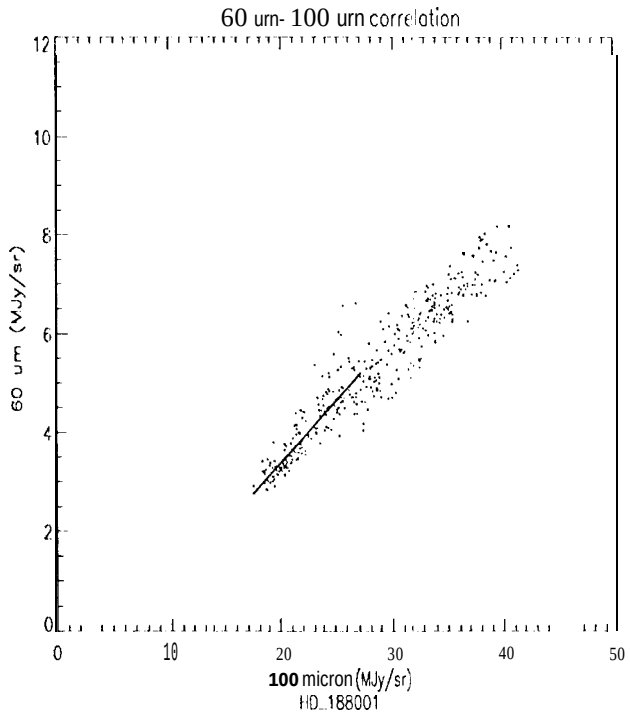
60 urn- 100 urn correlation
60 um (MJy/sr)
100 micron (MJy/sr)
HD_188001

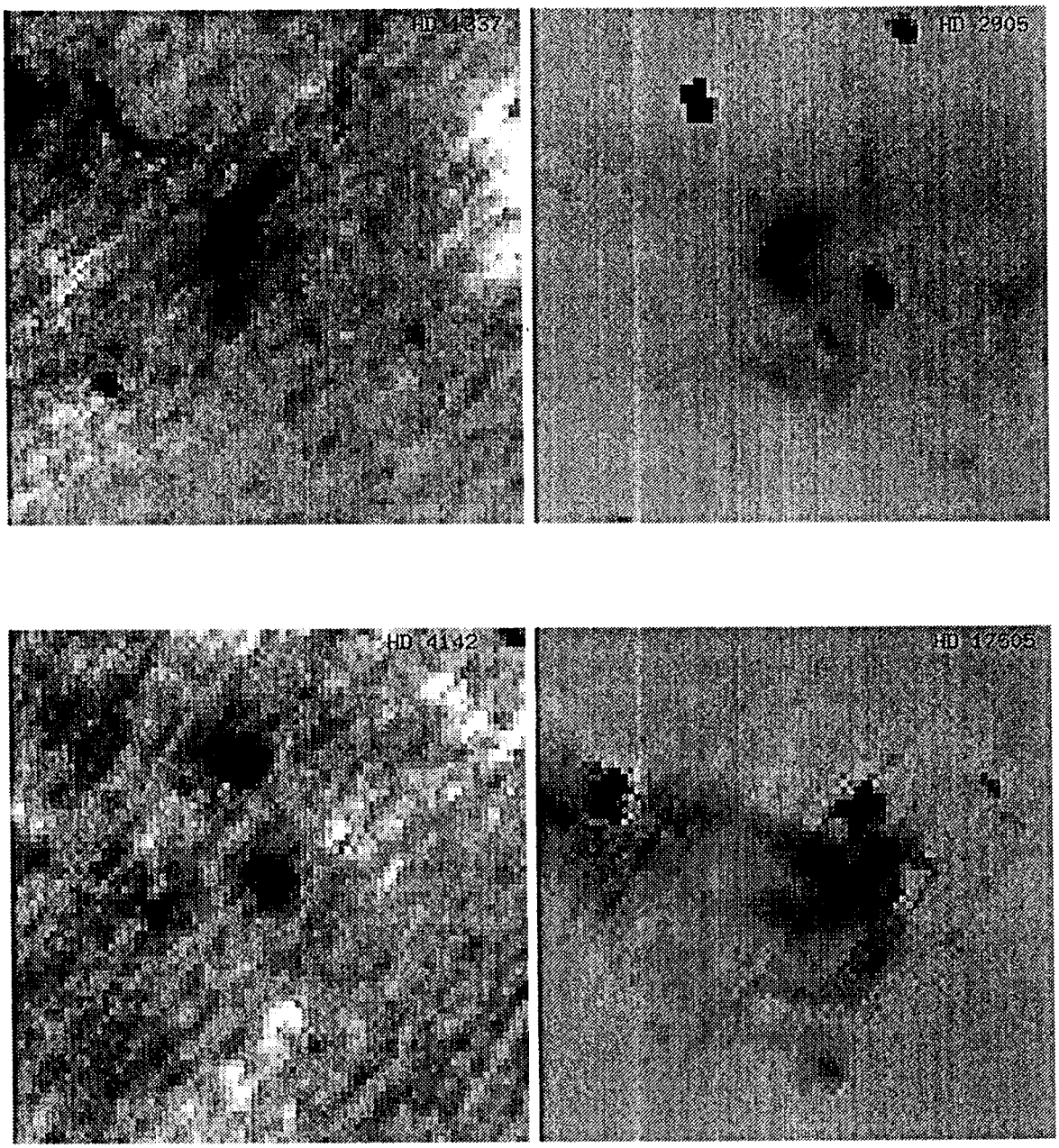

fig 2 (1/4)

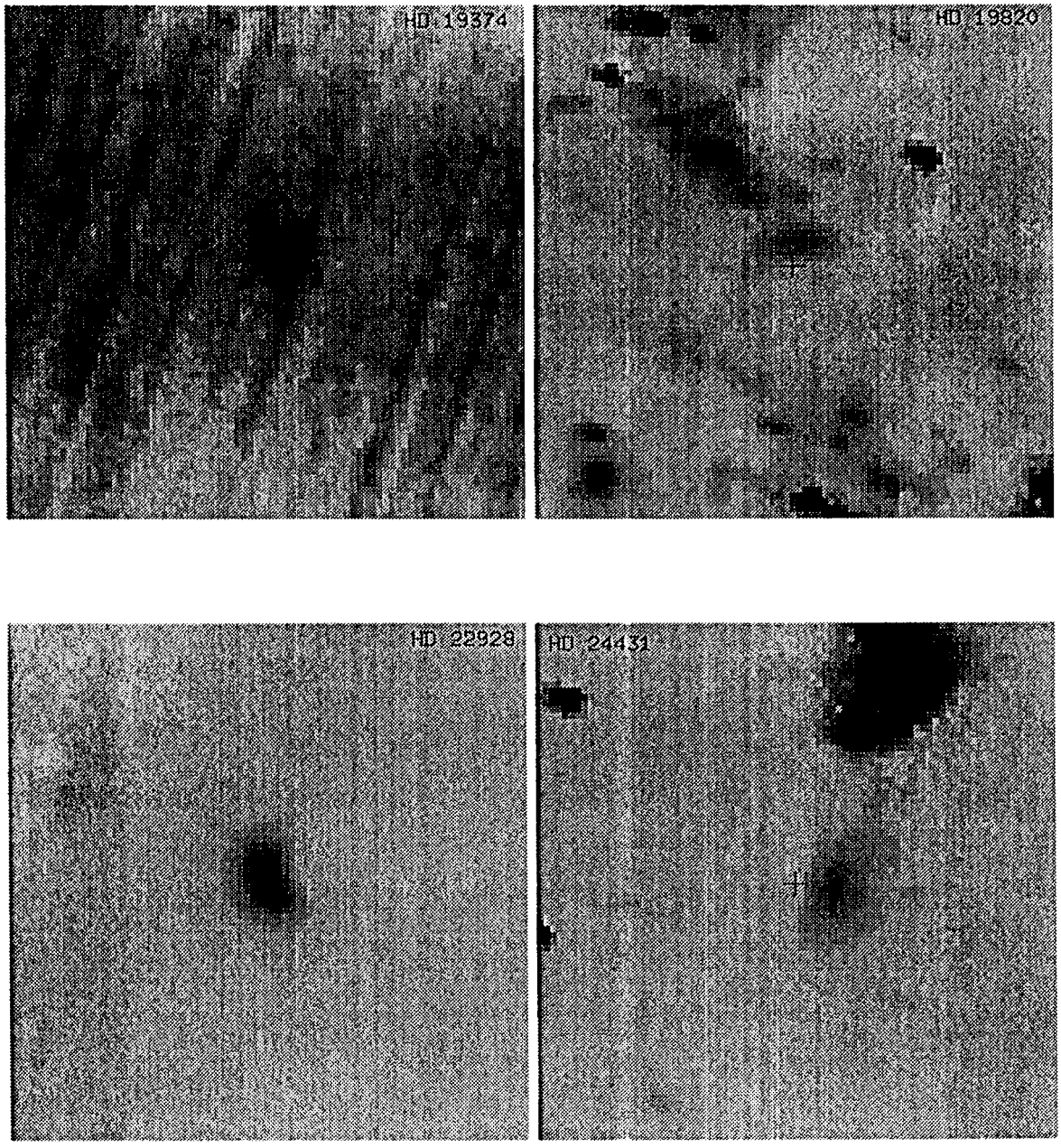

fig 2 (2/14)

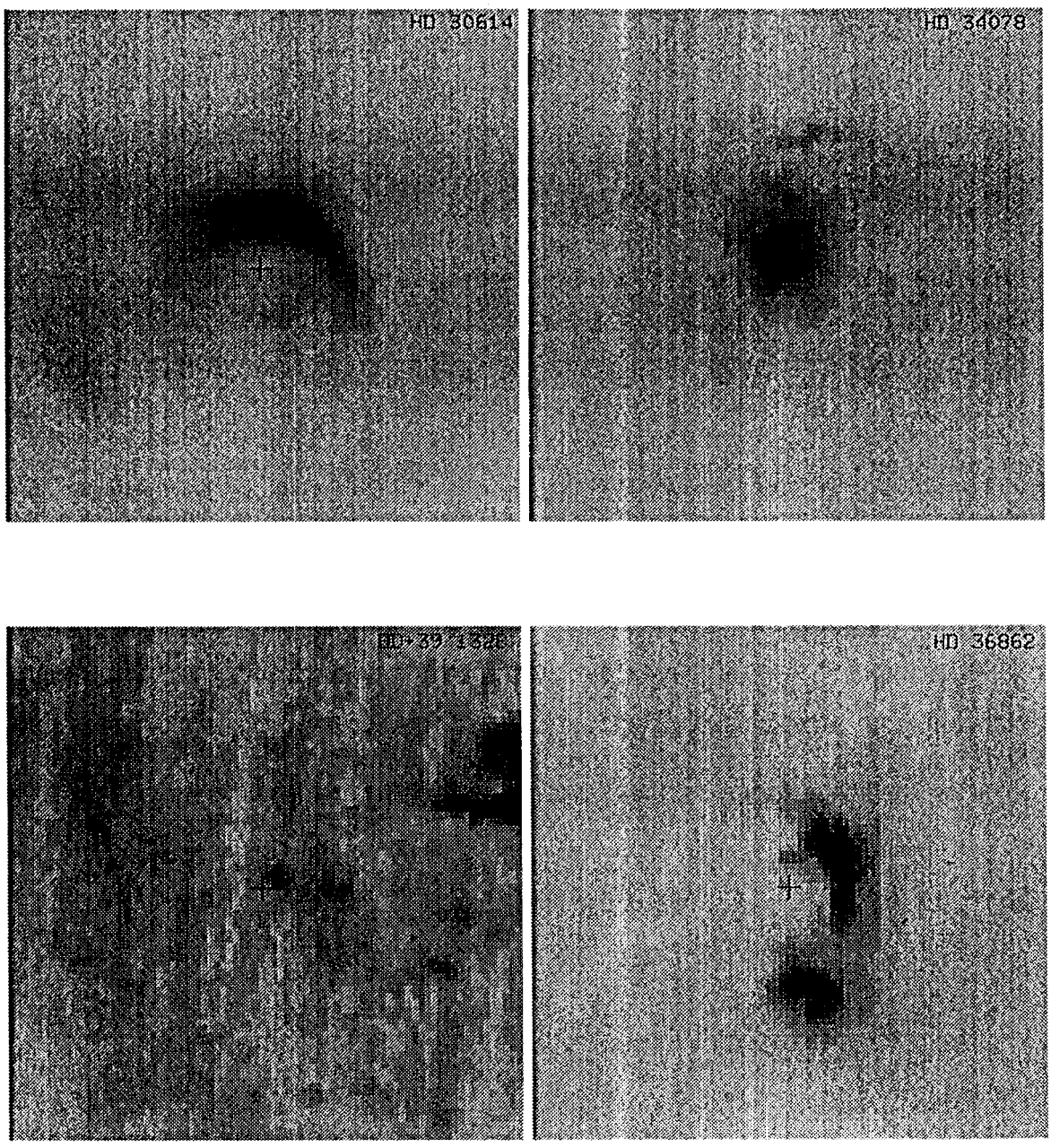

fig 2 (3/4)

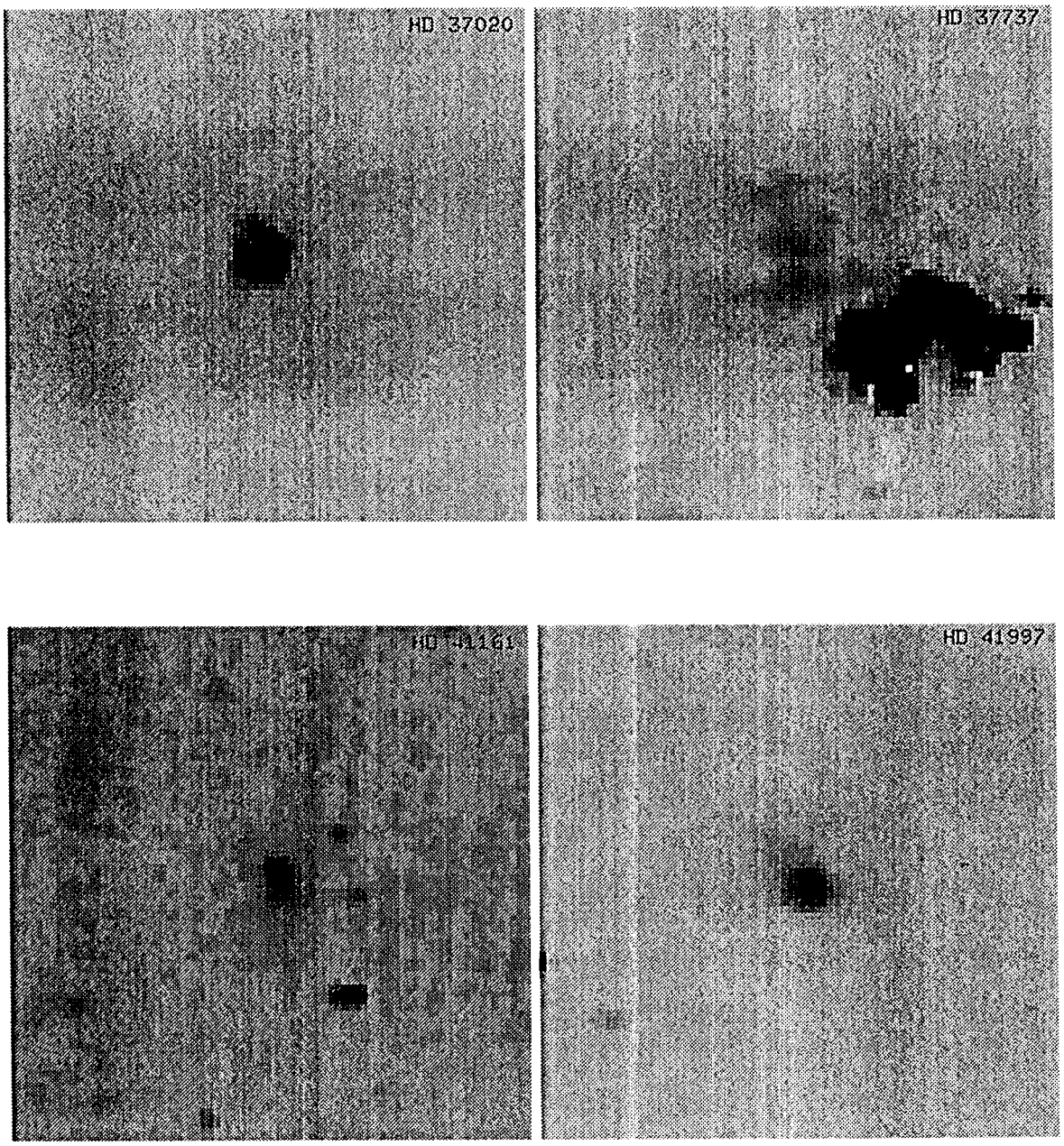

fig 2 (4/14)

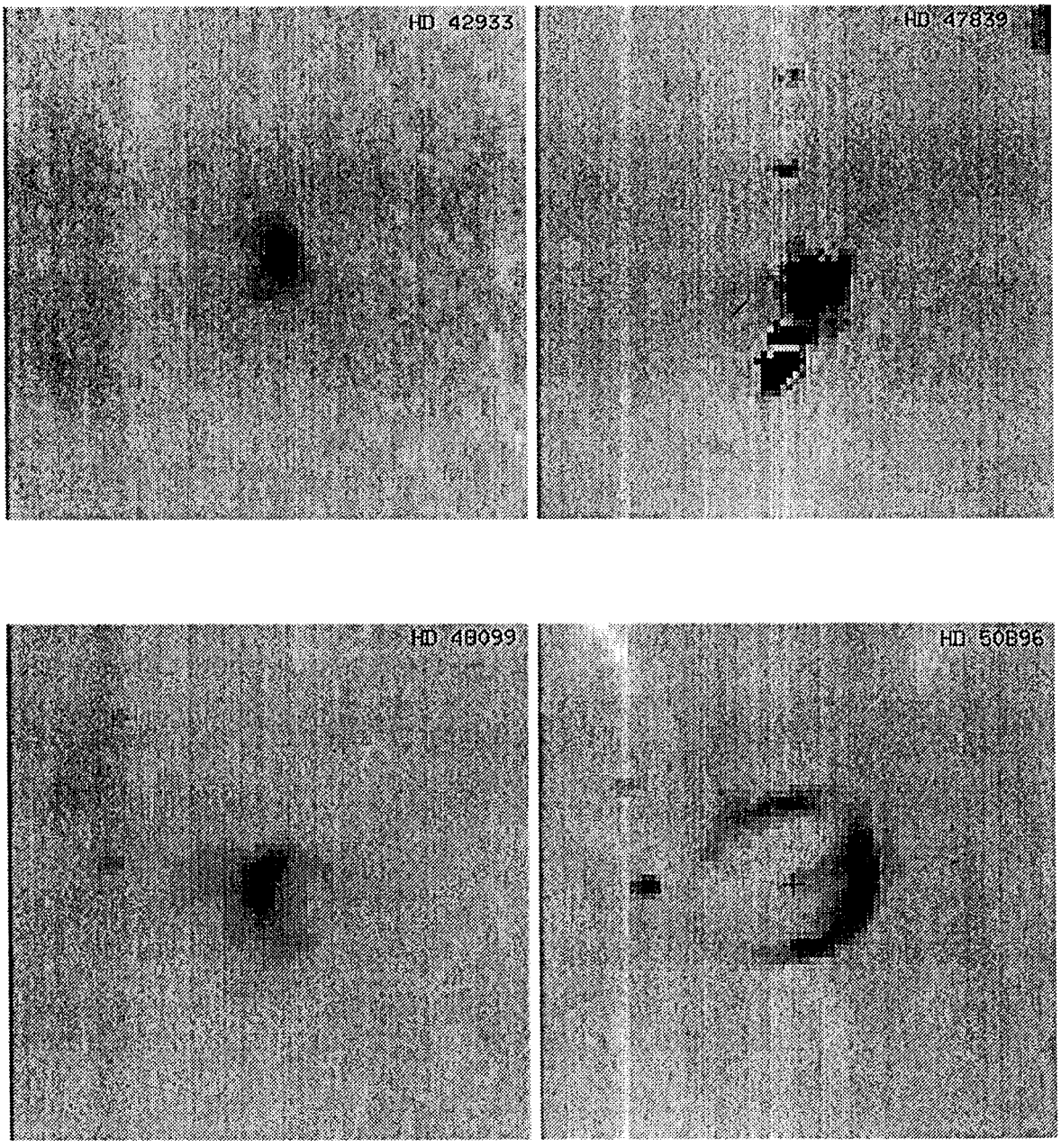

fig. 2 (3/14)

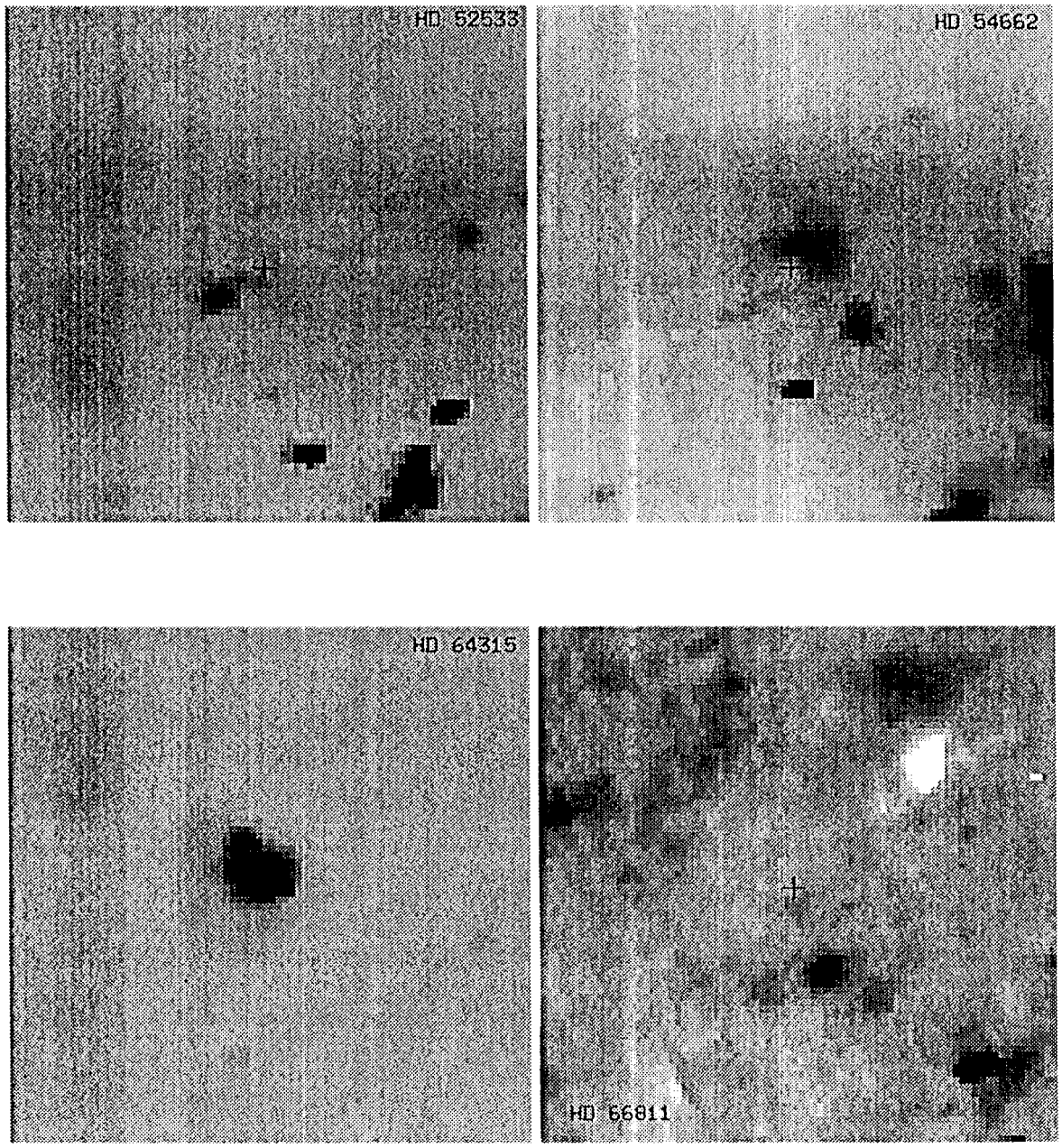

fig. 2 (6/6)

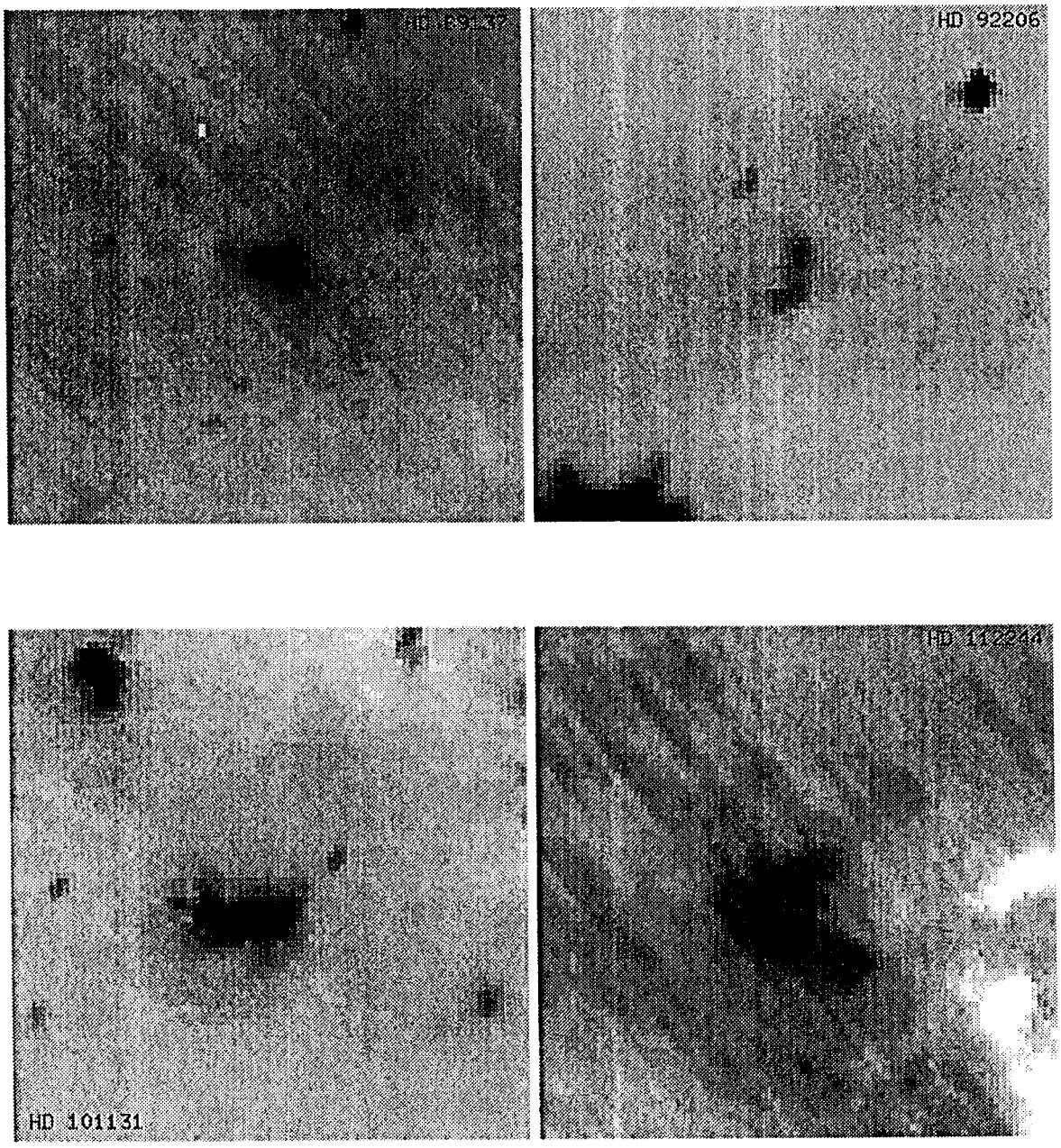

fig 2 (7/14)

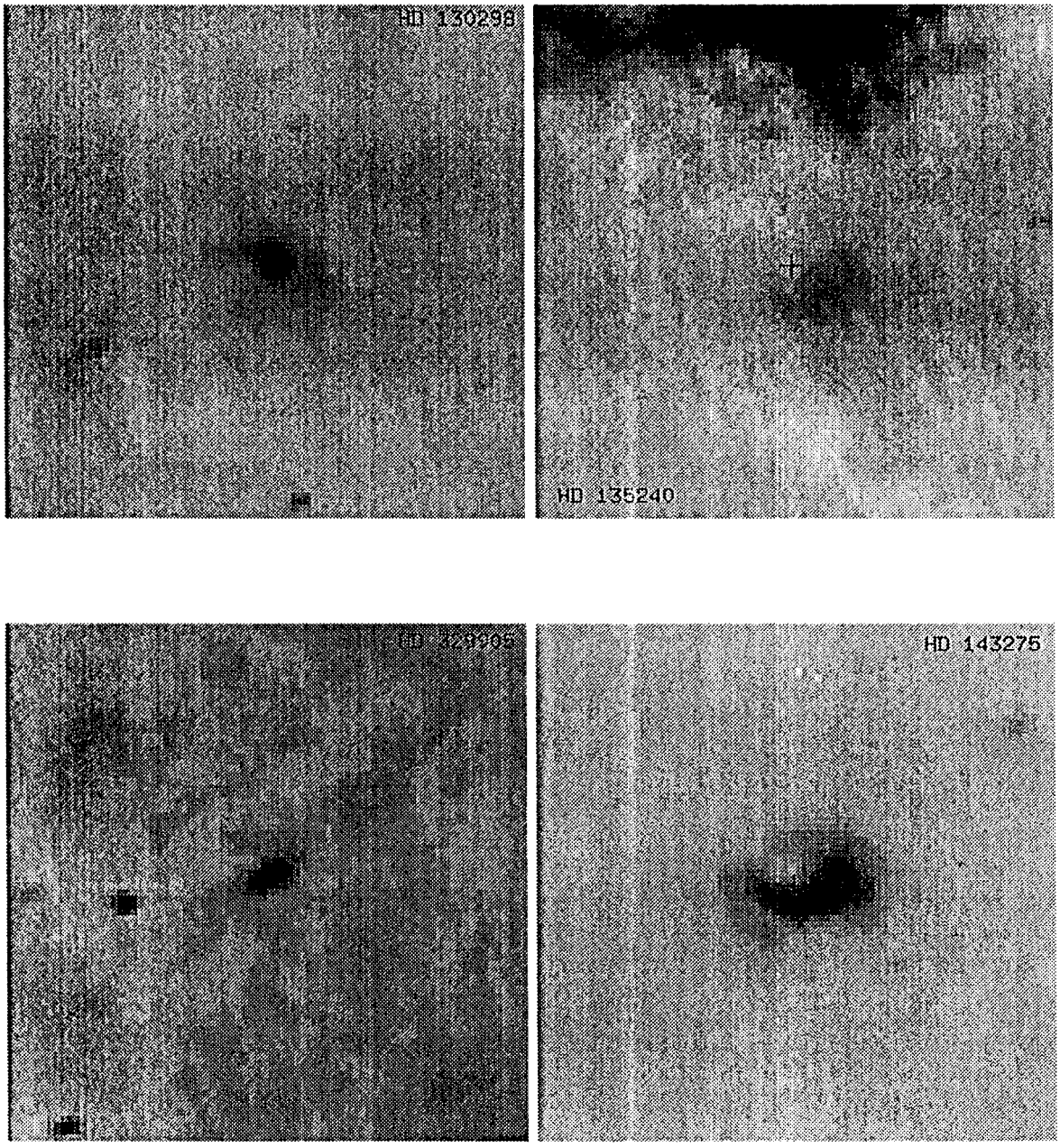

fig. 2 (8/14)

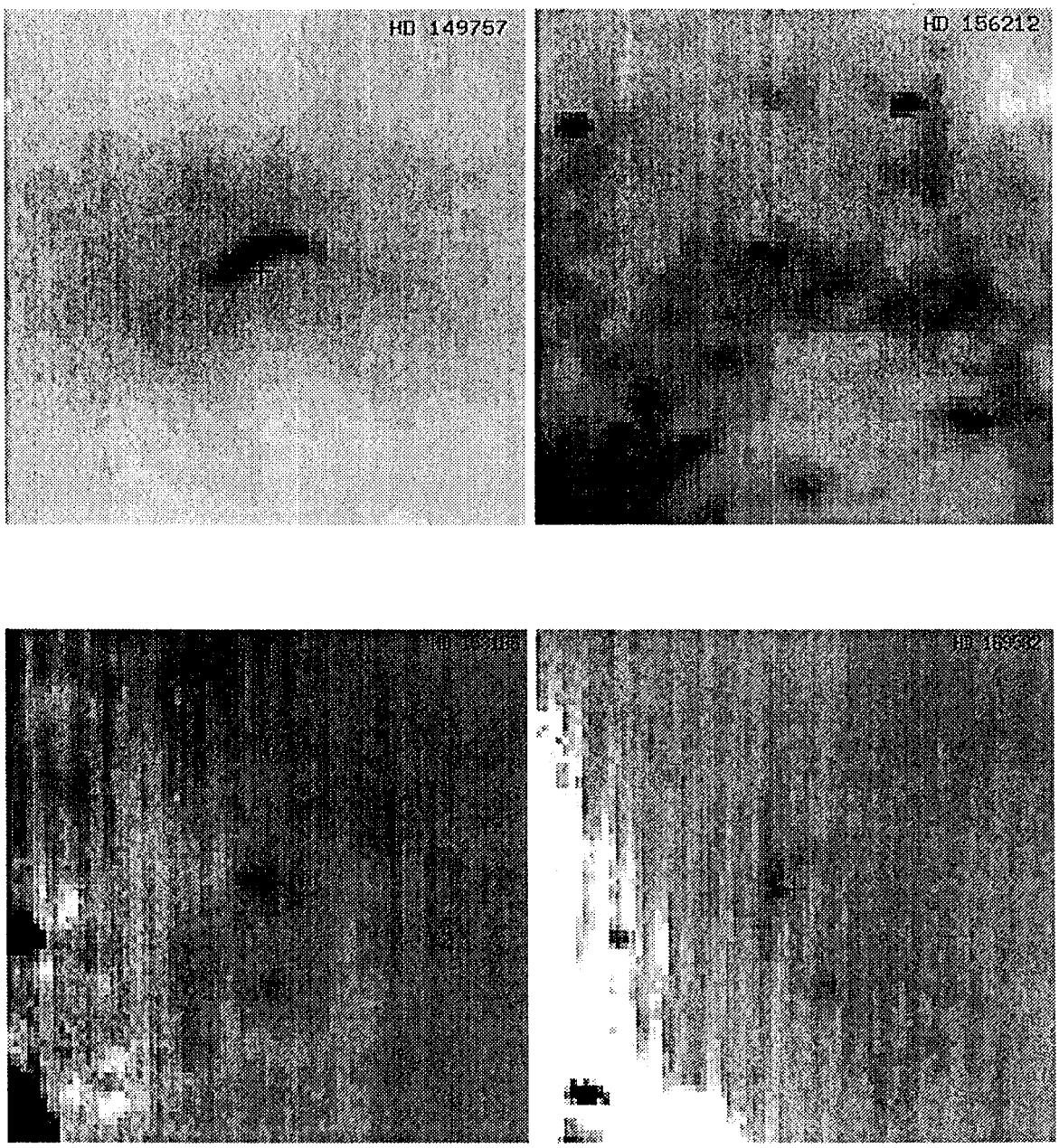

fig. 2

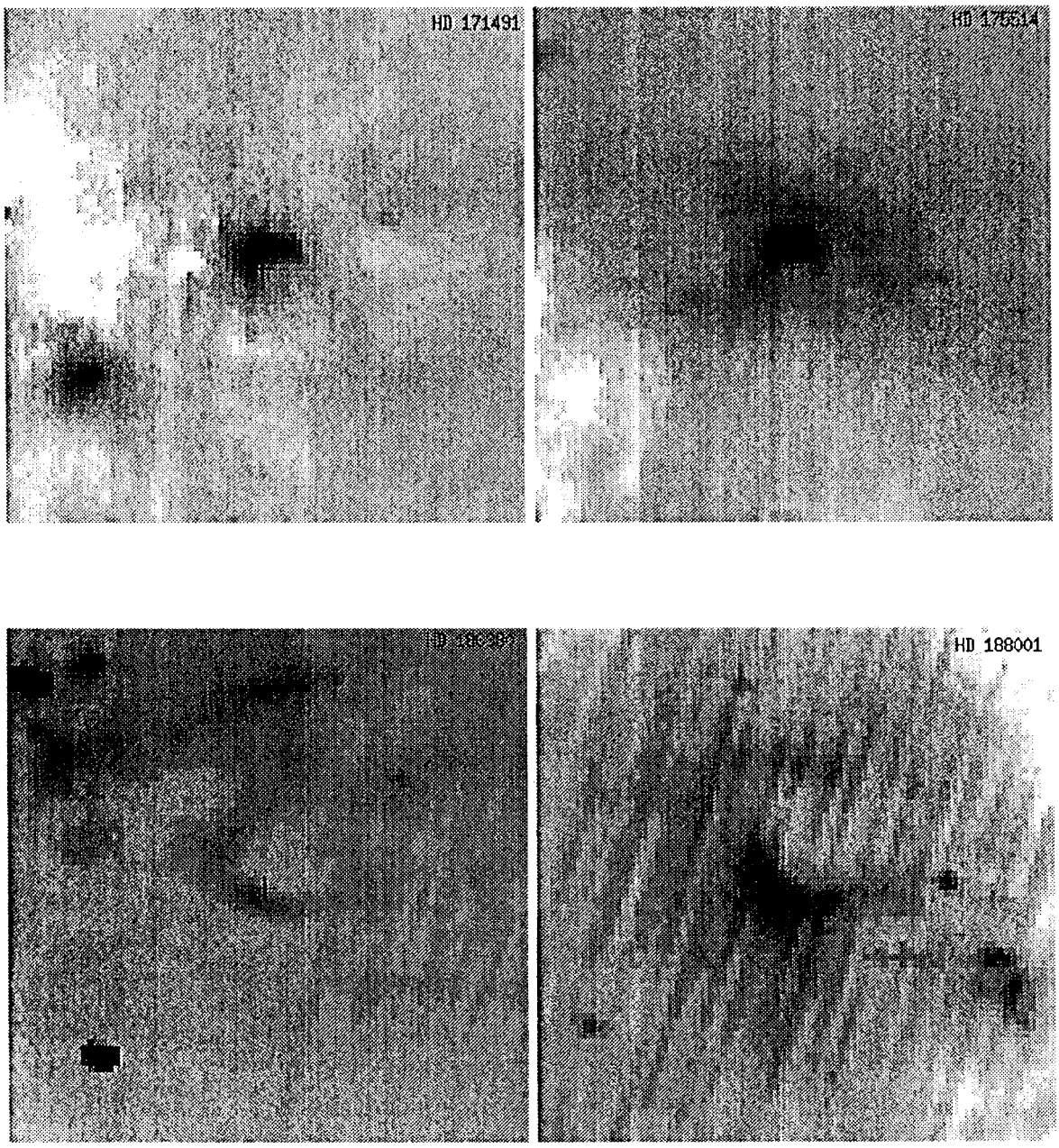

fig 2 (10/14)

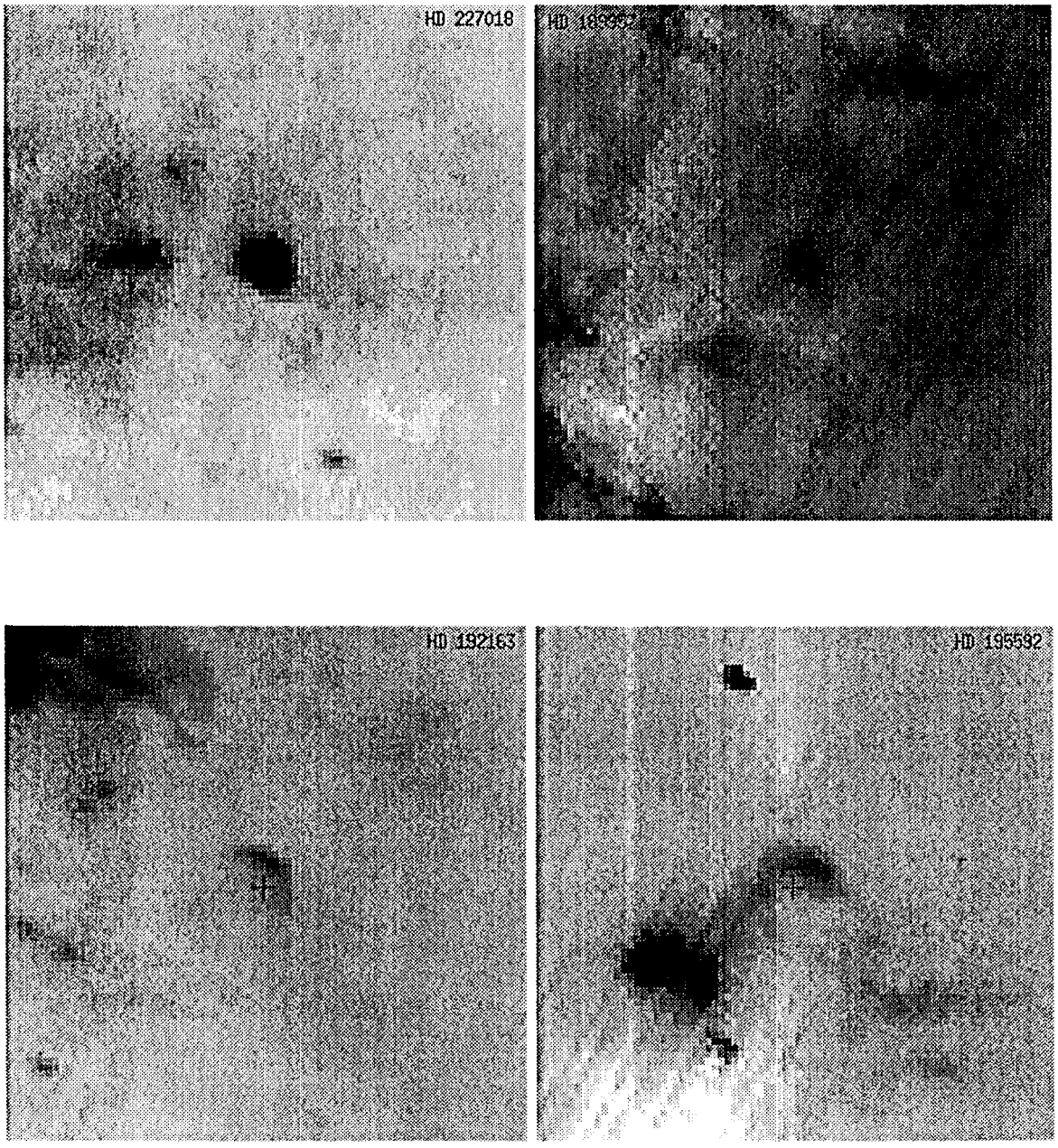

Fig.1 (rent) From the top, left to right: HD 227018, H]) 189957, HI) 192163, & HD 195592.

fig 2(H/...

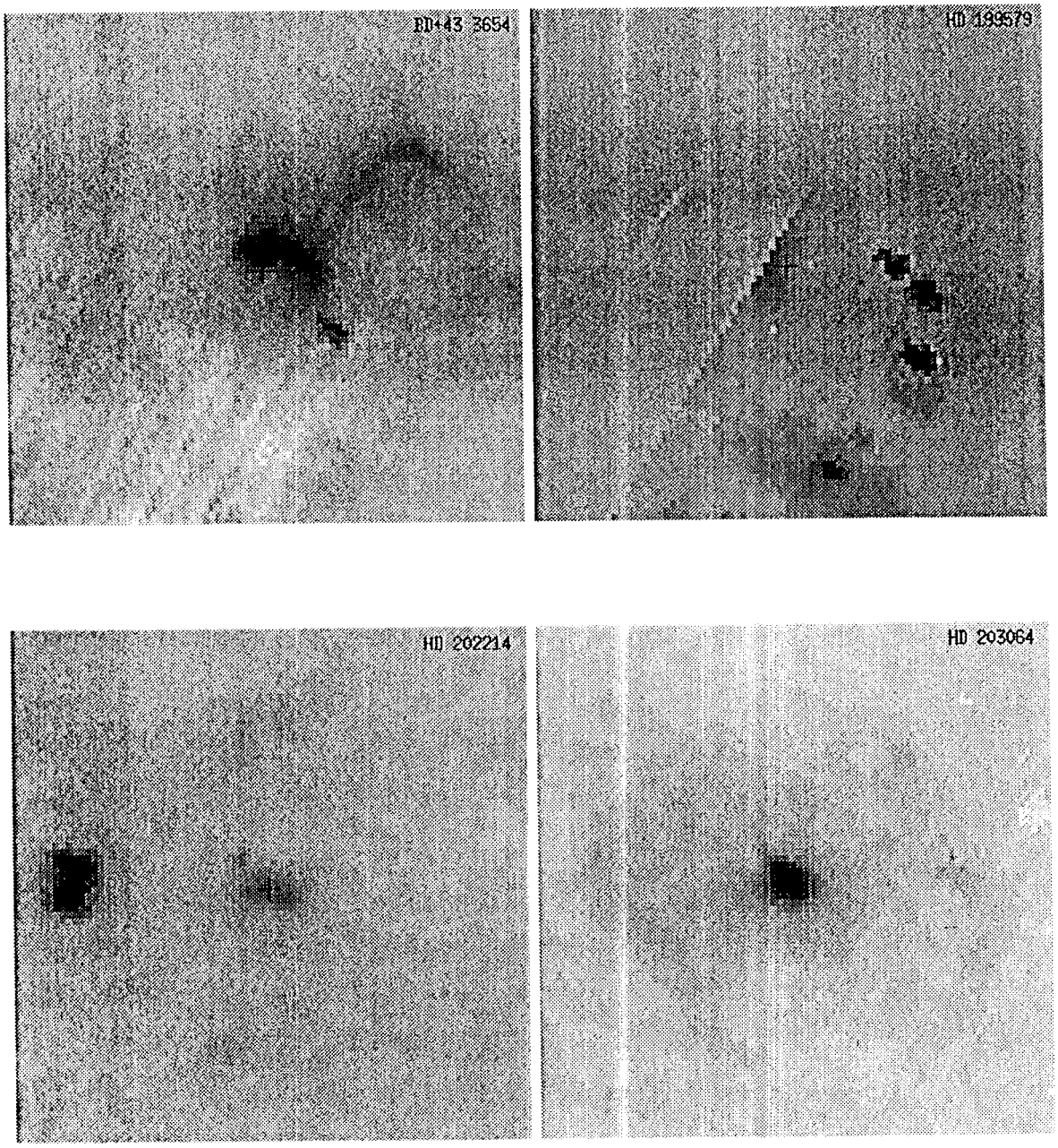

fig 2 (12/14)

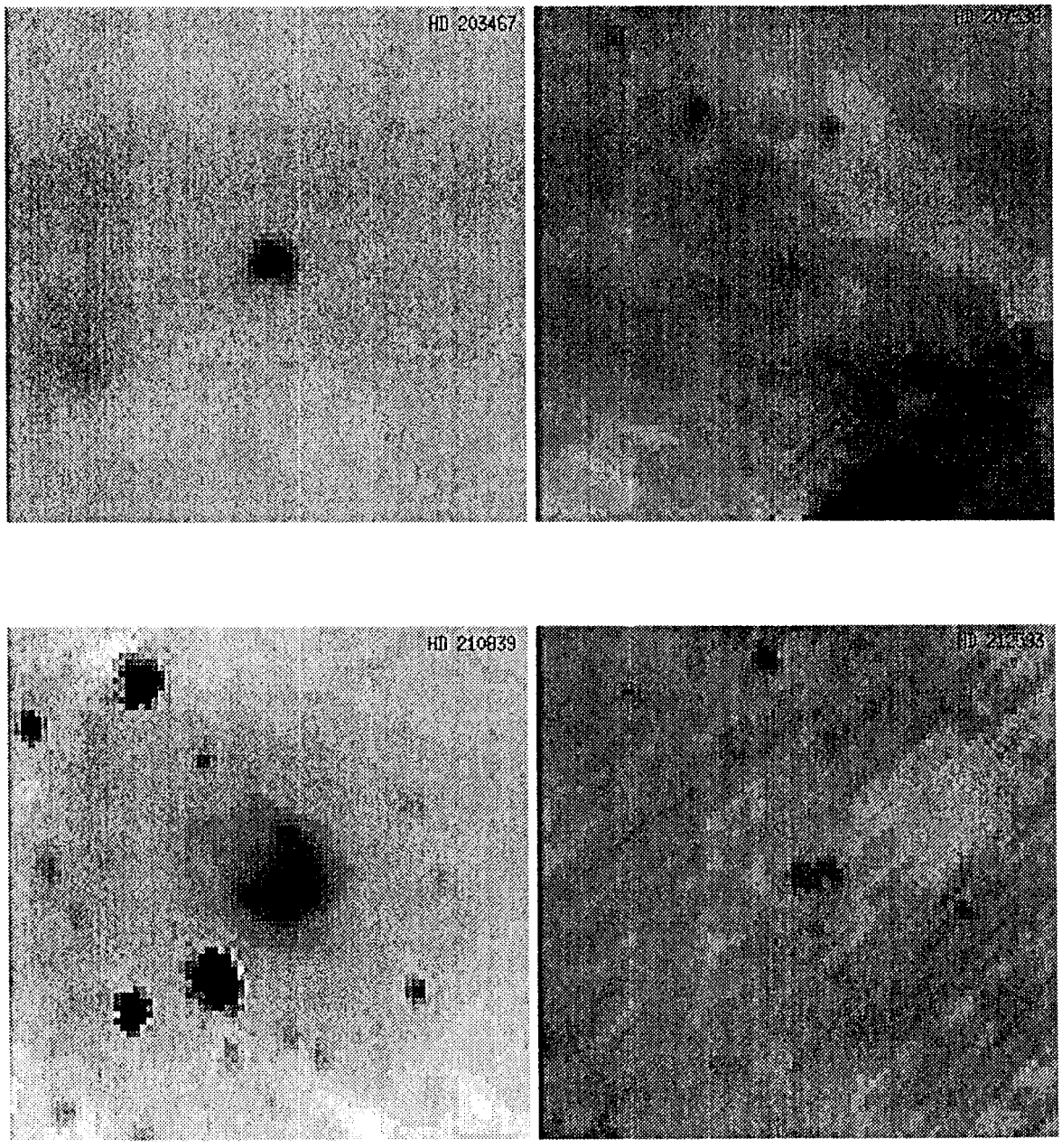

fig 2 (134 h)

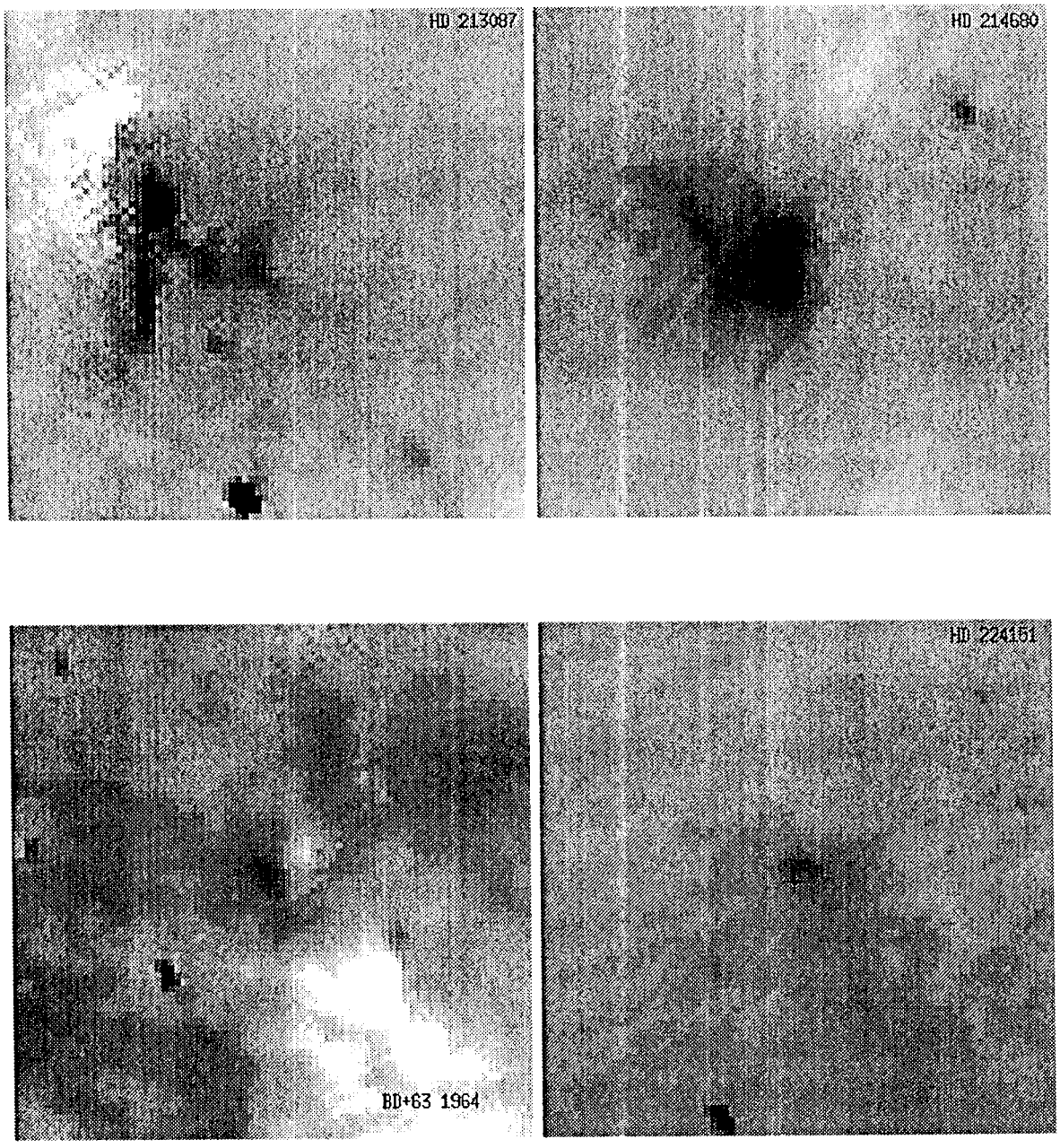

fig 2

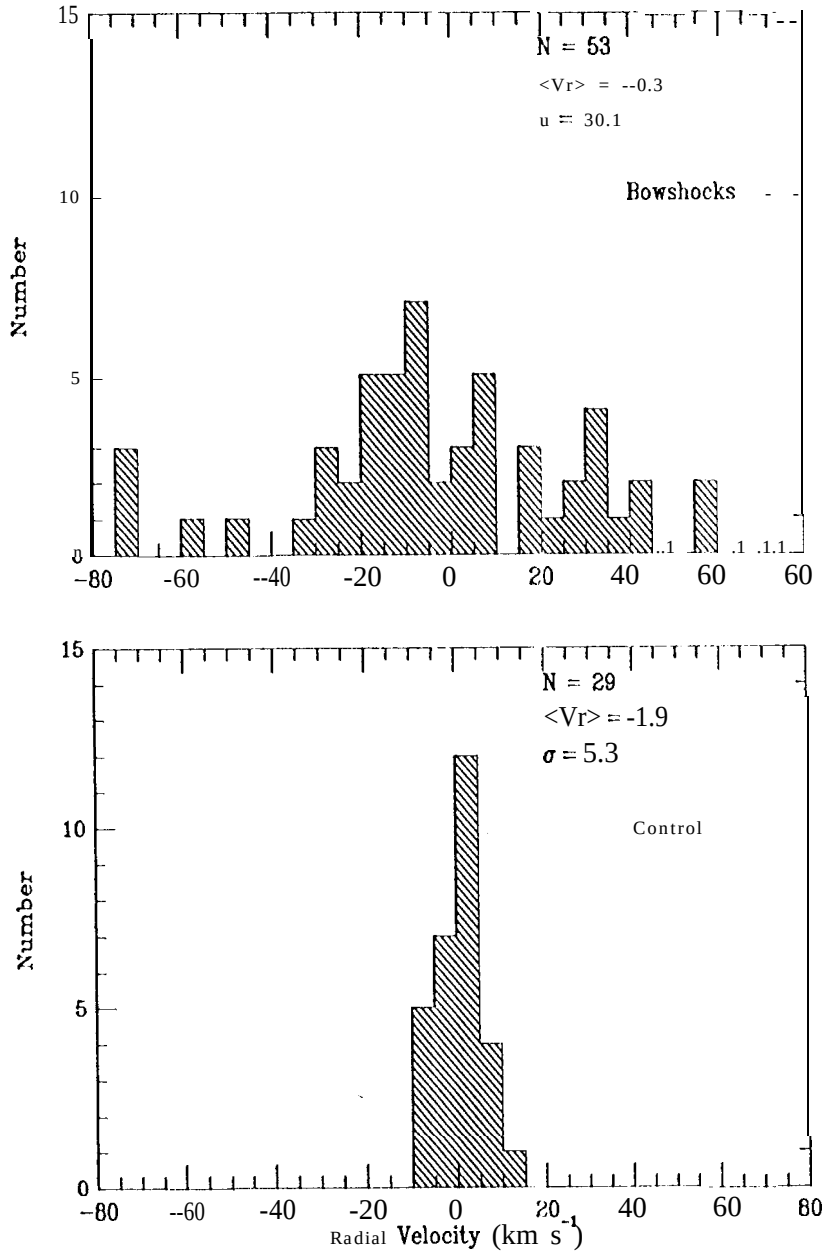
N = 53
<Vr> = --0.3
u = 30.1
Bowshocks
Number
N = 29
<Vr> = -1.9
σ = 5.3
Control
Number
Radial Velocity (km s-1)

fig 3

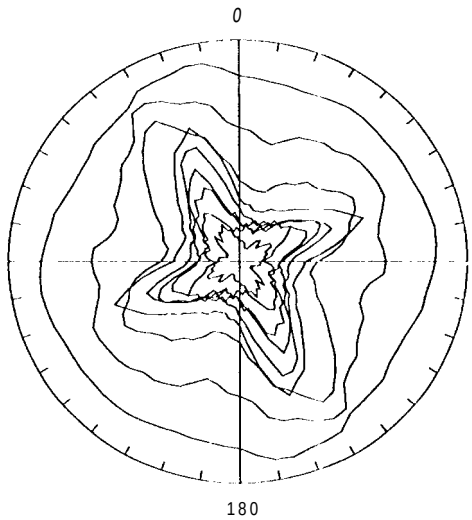

HD_ I 49757 band=3xradius= 15.0000

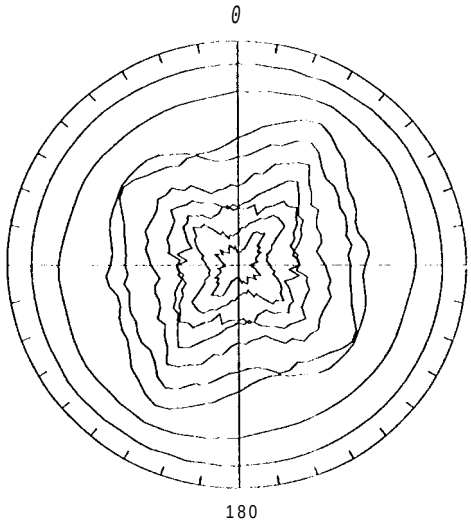

t{ D_188001band=3x radius= **15.0000**

fig. 4

90

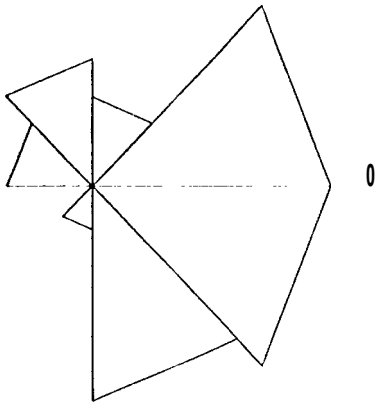

-90

Fig. 5